

Zürich, Switzerland, April 2011

SUPERCONDUCTING MICROWAVE FREQUENCY RING RESONATORS

Semester Thesis

Abstract

This thesis studies the behavior of microwave frequency ring resonators coupled capacitively to a coplanar transmission line. Ring resonators behave different to line cavities, since the electric field is produced by traveling instead of standing waves. This fact is of interest since the electric wave amplitude in a waveguide determines the coupling properties e.g. to a qubit, as it is carried out at the Quantum Device Lab at the Swiss Federal Institute of Technology. The goal of the thesis is the design and modeling of ring resonators at microwave frequency. Several models have been fabricated and one exemplary resonator has then been analyzed and compared to computational models.

Author: Ernst-Cornelius KOCH
Carried out at: Quantum Device Lab, Laboratory for Solid State Physics,
ETH ZÜRICH
Supervisor: Lars STEFFEN
Professor: Prof. Dr. Andreas WALLRAFF

Contents

1	Introduction	3
2	Theory	4
2.1	Waveguides	4
2.1.1	Coplanar Waveguides	5
2.2	Resonators	6
2.2.1	Resonance	7
2.2.2	Quality factor	7
2.3	Coupling	8
3	Computational Analysis	10
4	Measurements	12
4.1	Ring Resonator Fabrication	12
4.2	Measurement Technique	14
5	Results	15
5.1	Calibration	15
5.2	Resonator	16
6	Discussion	21
7	Conclusion	22
A	Designed Resonators	23
	Bibliography	24

1 Introduction

Nowadays computers all store information in bits of value 0 or 1. Quantum bits (qubits) can store information with value 0 or 1 as well, but also any superposition of them. To develop systems which can make use of the quantum mechanical properties of nature, has been the goal of many researchers, starting with Feynman [1] in 1982. In the last decade first models have been designed and were able to process simple calculations [2]. There are many candidates, including superconducting circuits, ion traps, semiconductor quantum dots and NMR, to process quantum computation. Superconducting electrical circuits is the one being chosen in this work.

The implementation as a superconducting coplanar waveguide (CPW) resonator has several advantages in cavity quantum electrodynamics (cQED), as capacitance, inductance can be well controlled [3, section I]. Fabrication of CPW transmission lines can be routinely realized these days with a very high precision (see section 4.1 on page 12).

The electrical circuit is realized by coplanar waveguides, and the qubits as cooper-pair boxes [3, section I]. A signal e.g. a photon is then sent in the circuit and supposed to couple with the qubit, to read-in or out information. To enhance coupling probabilities the photon could pass by the cooper-pair box, which acts as the q-bit, many times. This can be realized by using a resonator as quantum bus. The bus can thereby also be used to entangle two or more qubits. The properties of the resonator then influence strongly the coupling between the input signal and qubit. Different resonator designs are therefore to be studied. The resonator is basically defined by its length and its Q-factor. Especially the Q-factor is not always easy to calculate beforehand as we will see later on.

This work will describe and present several suggestions of potential setups. In section 2 the theoretical background is being given. A computational analysis of simulated ring resonators is being performed using the programs *Mathematica*, *Microwave Office* and the finite-element simulation *Maxwell12* in section 3. Section 4 describes the experimental measurement setup used for this experiment. In section 5 the results of the experiments will be presented and the last sections discuss and compare the results.

2 Theory

2.1 Waveguides

An optical waveguide is an dielectric element embedded in dielectric material of smaller refractive index n . An electro-magnetic wave will be reflected at the boundaries due to the distinct refractive indices without emerging to the surrounding media. The material and design determine the supported modes of a waveguide. Those are transversal waves which are self-consistent in a way, that after being reflected twice they are in phase with themselves again.

$$k_{ym} = m \frac{\pi}{d} \quad (1)$$

with k being the specific wavenumber in direction y , m the mode number and d the separation between the boundaries.

A typical complex amplitude, of a wave traveling in direction y , with an electric field in z direction, can be described by

$$E(y, z) = a_m u_m(y) e^{i \beta_m z} \quad (2)$$

with

$$\begin{aligned} \beta_m &= \sqrt{k^2 - k_{ym}^2} \\ u_m(y) &= \sqrt{\frac{2}{d}} \cos(m\pi \frac{y}{d}), \quad m = 1, 3, 5, \dots \\ u_m(y) &= \sqrt{\frac{2}{d}} \sin(m\pi \frac{y}{d}), \quad m = 2, 4, 6, \dots \end{aligned}$$

where a_m is the maximal amplitude, u_m the complex envelope, that has to fulfill the Helmholtz equation and be at zero amplitude at the boundaries, and β the propagation constant.

The spectrum of waveguides is seemingly endless but in this work we will focus on one dimensional, super conducting coplanar waveguides.

2.1.1 Coplanar Waveguides

A coplanar wave guide (CPW) consists of conductors on a dielectric surface. The actual wave guide is a center strip conductor which is surrounded by adjacent conducting ground planes.

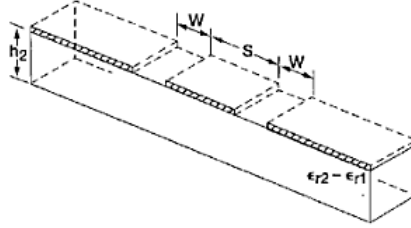


Figure 1: Schematic of a Coplanar Wave Guide (Picture from [4])

The conductors are of neglectable thickness, such that waves can only exist in the plane. To characterize a co-planar wave guide entirely, impedance Z_0 and the effective dielectric constant ϵ_{eff} have to be determined. Analytically this can be done by solving [4]:

$$\epsilon_{\text{eff}} = \frac{1 + \epsilon_r \frac{K(k')}{K(k)} \frac{K(k_3)}{K(k'_3)}}{1 + \frac{K(k')}{K(k)} \frac{K(k_3)}{K(k'_3)}} \quad (3)$$

$$Z_0 = \frac{60\pi}{\sqrt{\epsilon_{\text{eff}}}} \frac{1}{\frac{K(k)}{K(k')} + \frac{K(k_3)}{K(k'_3)}} \quad (4)$$

with,

$$K(k) = \int_0^{\pi/2} \frac{d\Theta}{\sqrt{1 - k^2 \sin^2(\Theta)}}$$

$$k = a/b, \quad k' = \sqrt{1 - k^2}, \quad k_3 = \frac{\tanh(\pi\alpha/2h)}{\tanh(\pi\beta/2h)}, \quad k'_3 = \sqrt{1 - k_3^2}$$

where $a = S/2$ and $b = (S + W)/2$ which can be identified in fig. 2.1.1.

In a medium with the effective dielectric constant ϵ_{eff} the effective velocity, with which an electromagnetic wave travels, can be expressed as

$$v_{\text{eff}} = \frac{c_0}{n}, \quad n = \sqrt{\epsilon/\epsilon_0}$$

where c_0 is the speed of light in vacuum, n is the refractive index and ϵ_0 is

the vacuum permittivity.

If the electric length L_e is being understood as the wavelength in vacuum λ , the corresponding length of the transmission line can be calculated as

$$L = \frac{\lambda \cdot c_0}{\sqrt{\epsilon_{\text{eff}}}} \quad (5)$$

Using CPWs is advantageous since they can be fabricated easily and on micro-scale precision (see section 4.1 on page 12). That way resonators (see section 2.2) with q-factors of up to a couple hundred thousands can be produced.

2.2 Resonators

The resonator confines light to its structure and stores certain frequencies, determined by its setup. Photons in the resonator can be seen as trapped in it, either by being reflected back and forth between mirrors or circulating in the confinement. Therefore wave functions of many photons overlap constructively, when introduced with certain frequencies. Due to the frequency storing property, the resonator is the part of the quantum system (see section 1 on page 3), to which the qubit is coupled. So, a photon has a greater possibility to interact with the qubit.

A resonator consists of optical elements that allow standing waves to evolve in them. A famous example is the Fabry-Pérot-Resonator which is made of two parallel mirrors between which light is reflected. This work though, explicitly examines the behavior of circular CPW transmission line resonators. The properties of a resonator are basically described by its resonance frequency, and the quality factor, which are described more detailed on the next page.

Figure 2: Fabry-Pérot-Resonator [5]

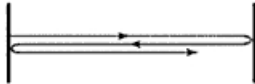


Figure 3: Integrated Ring Resonator [5]



2.2.1 Resonance

Photons in an optical resonator will feel a phase shift after one round trip. If the wave function is at resonance, the phase shift after one round trip will be equal to 2π , so that constructive interference occurs. For a wave traveling with phase velocity $c/\sqrt{\epsilon_{\text{eff}}}$ the resonance condition therefore reads:

$$f_q = \frac{c}{\epsilon_{\text{eff}}} \frac{1}{L} \cdot q, \quad q = 1, 2, \dots \quad (6)$$

where f , denotes the frequency, c the speed of light, ϵ_{eff} the effective electric permeability and L the length to complete one round trip, e.g. $2d$, for a Fabry-Pérot-Resonator of length d , respectively l for a ring resonator of length l .

To introduce Photons into the resonator one possibility is to capacitively couple the resonator transmission to a second, stimulating transmission line. By the coupling between the transmission lines a frequency shift is induced, because standing waves in the resonator interfere with the evanescent electromagnetic waves from the stimulating transmission line.

2.2.2 Quality factor

The quality factor, Q , is defined as stored energy in the cavity divided by the energy loss per cycle times 2π . For a cavity of sufficiently high reflectivity, this can be reduced to:

$$Q = \frac{f_q}{\Delta f} \quad (7)$$

where Δf is the full width at half maximum of the resonance [5]. Thus for a high q-factor cavity the losses in a resonant system are low, which can be directly related to the photon life time in the cavity [5],

$$\tau = \frac{Q}{2\pi \cdot f_q} \quad (8)$$

Whereas the resonance frequency is mainly dependent on the resonator length, the q-factor is mainly dependent on the coupling. In this experiment the resonator is coupled capacitively to a stimulating transmission line, in a way that photons can enter the optical cavity. Since the capacity cannot easily be calculated a finite-element calculation will be used (see section 3 on page 10). To confine the coupling only to a part of the ring resonator and reduce coupling of the other parts, the ring is not designed circular, as you can see in A on page 23. Even though resonances might appear in a more complicated way, ring resonators can have advantages over line resonators. A monochromatic wave in the resonator can be expressed as (see [5])

$$U(\mathbf{r}, t) = \Re \left\{ U(\mathbf{r}) e^{i2\pi f t} \right\} \quad (9)$$

with $U(\mathbf{r})$ the complex amplitude envelope function.

For a line resonator these bounding conditions define strictly where amplitude maxima and minima are positioned for each current. The ground mode for the Fabry-Pérot resonator of length d e.g. has amplitude minima at the mirrors and a maximum at $x = d/2$. A maximum for the ground mode at $x = d/4$ can not exist. For ring resonators on the other hand the constraint of amplitude in propagation direction does not exist. Amplitudes of standing waves can be freely distributed in the resonators. This is desirable, since the coupling of qubits is depended of the amplitudes. Using a ring-resonator the qubits could theoretically be placed anywhere within the resonator, without diminishing the coupling strength.

2.3 Coupling

If two waveguides are close enough to one another their electric field amplitudes can overlap. This overlapping actually induces a field in the adjacent waveguide, which can now travel through the partnering waveguide, or, in

case of a non negligible preexisting wave, modulate its amplitude and phase. The resonator can so with be coupled capacitively to an stimulating transmission line.

Since the interaction is distributed over the whole coupling zone, the shift is dependent on geometry and the strength of the coupling [6]. However, to diminish the shift a long, weak coupling is favorable over a short, strong coupling region as it has been shown by Popovic et al [6].

Even though an exact solution of the electric fields in the transmission lines could be found by solving the maxwell equations, an approximation for the resonance frequency and quality factor can be made by representing the cavity as a lumped element, parallel LCR oscillator (see fig. 4)

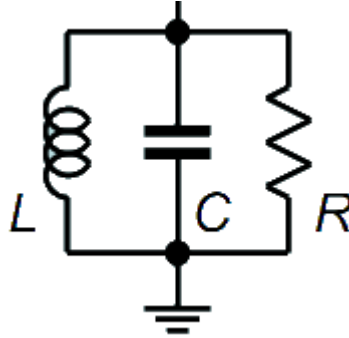


Figure 4: Parallel LCR oscillator

, as it has been done in [7] for a symmetrically coupled line resonator. The impedance of the resonator can then be calculated as

$$Z_{LCR} = \left(\frac{1}{i\omega L} + i\omega C + \frac{1}{R} \right)^{-1}$$

where L , C and R are the inductance, capacitance and resistance of the resonator. The resulting internal resonance frequencies ω_n ($n=1$ for the fundamental mode) and internal quality factor Q_{int} can then be retained as:

$$\omega_n = 1/\sqrt{L_n C}$$

$$Q_{\text{int}} = \omega_n R C$$

It can be shown ([7]) that the internal resonance frequency is shifted due

to the capacitive coupling to a resulting resonance frequency of

$$\omega_L = 1/\sqrt{L_n(C^*)} \quad C^* > 0$$

$$Q_L = \omega_n \frac{1}{1/R + 1/R^*} C \quad R^* > 0$$

In this experimental thesis we will model several rings and solve for the characterizing parameters numerically by i) calculating the effective coupling capacitance using the finite-element simulation *Maxwell12* and ii) by solving for the parameters directly with *Microwave Office*.

3 Computational Analysis

Eight resonators have been fabricated and simulated beforehand. They can be grouped into resonators with direct coupling (RR500d4, RR500d6, RR500d9, RR100d9), with no ground plane between the transmission lines of resonator and stimulated center conductor, and ones with indirect coupling (RR1500i4, RR500i4, RR500i5, RR500i2), having a ground plane in between them. All designs are represented in the Appendix.

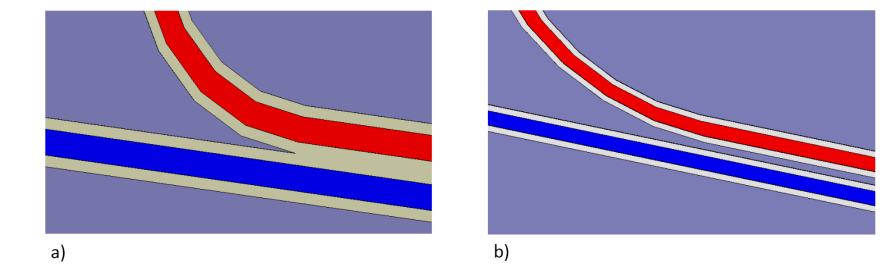


Figure 5: a) direct coupled resonator b) indirect coupled resonator

In the simulations, capacities have been calculated with *Ansoft's Maxwell 12*, then Q-factors and resonances have been calculated using *Microwave Office*. First the capacities were examined using a finite-element technique. Conductors were assumed to be perfect conductors with a relative permeability of 1 and were placed on a theoretical sapphire grounding of relative permeability equal to 10. The adjacent ground planes were assumed to be perfectly grounded. The results can be seen in Tab. 1 on the following page.

Resonator	Capacity [pF]	abs. Error	rel. Error
RR1500i4	0.023	± 0.002	10%
RR500i2	0.011	± 0.001	10%
RR500i4	0.0086	± 0.0009	10%
RR500i5	0.0077	± 0.0008	10%
RR500d4	0.036	± 0.004	10%
RR500d6	0.029	± 0.003	10%
RR500d9	0.022	± 0.002	10%
RR100d9	0.0063	± 0.0006	10%

Table 1: Calculated capacities of fabricated resonators

Determining the resonances only from the so calculated capacities would ignore the structure of the resonators and their exact design. So the q-factors and frequencies captured in the resonator were simulated with Microwave Office. Shown in table 2 are resonances and q-factors of the fundamental mode. We can see a resonance by not transmitted input signals. If the input signal is at resonance with the resonator, it will excite the ring and stay there for the photon lifetime τ , reducing transmission. As we can see in fig. 7 on page 13, direct coupled resonators eventually show a double peak. In this case the more developed resonance is being given. To determine the q-factor and the resonance frequencies the gap has been modeled in Microwave Office, using a coplanar linestrip element with an impedance of 50Ω . The resulting transmission spectra of the calculation have than been used to calculate the q-factors by using formula 7 on page 7. A representative peak of the RR500d4 Resonator is shown in fig. 6 on the following page.

Resonator	Resonance Frequ. [GHz]	rel. Error	Q-factor	rel. Error
RR1500i4	7.19401	1%	2186	1%
RR500i2	7.19828	1%	16000	5%
RR500i4	7.19789	1%	25700	8%
RR500i5	7.19805	1%	31300	10%
RR500d4	7.19592	1%	1950	1%
RR500d6	7.20767	1%	3125	1%
RR500d9	7.21799	1%	4825	1%
RR100d9	7.20368	1%	125000	1%

Table 2: Calculated q-factors and resonances of fabricated resonators

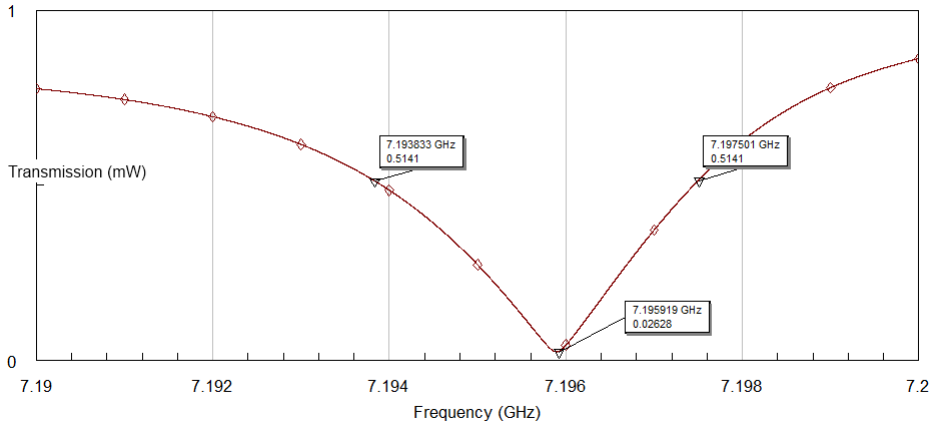


Figure 6: Transmission at resonance frequency of RR500d4

An exemplary entire spectrum of direct and indirect coupled resonators can be seen in figure 7 and figure 8, page 13.

4 Measurements

4.1 Ring Resonator Fabrication

The experiment was performed with a superconducting 1D transmission line resonator as cavity. It consists of an isolated Niobium center conductor of width $t = 10\mu\text{m}$, which is surrounded by $4.5\mu\text{m}$ distant adjacent planes. The center conductor and the planes are made of $t = 150\mu\text{m}$ thick Niobium layers. The conductors are fabricated on high-resistant, $h_2 = 500\mu\text{m}$ thick sapphire wafers, as elaborately described in [7, section II].

To process the waveguides a chromium coated quartz glass mask is designed, containing information of the desired gaps between the center conductor and adjacent planes. The wafer consists of a niobium coated sapphire substrate. To begin the procedure a photo resist layer is added to the wafer. Then the fabricated mask is placed above the wafer. Exposing the setup to the light of an optical lithography lamp will now break the photo resist layer at the unshaded locations. A developing bath then washes out the remaining broken photo resistor structures on the light-exposed sapphire wafer spots. Left behind is now the niobium layer at the washed out positions. Ion etching and cleaning ensures that previously shaded regions stay fixed

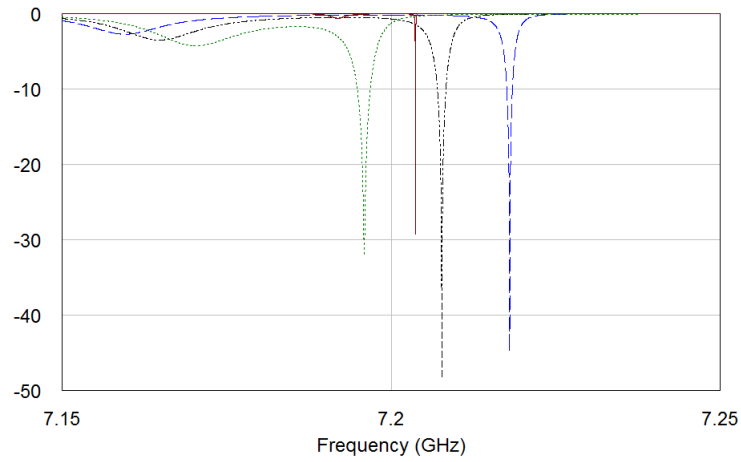


Figure 7: Transmission at induced frequency in dB. Dotted, green: RR500d4 - Full, red: RR100d9 - Dot striped, black: RR500d6 - Striped, blue: RR500d9

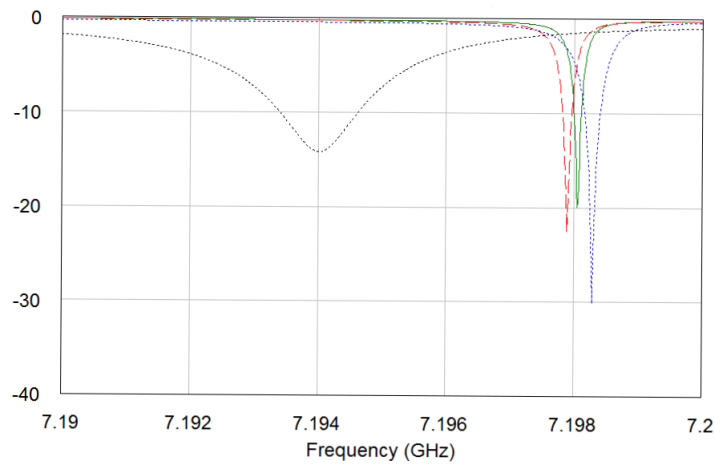


Figure 8: Transmission at induced frequency in dB. Dotted, black: RR1500i4 - Striped, red: RR500i4 - Full, green: RR500i5 - Dotted, blue: RR500i9

but the exposed niobium layer is removed from the substrate. Washing and removing the remaining photo resistant layer now leaves behind the desired microchips. The wafer, which usually contains more than one microchip, is then diced into individual chips. Each chip is then being glued onto a printed circuit board (PCB) and its conducting plates bonded to the PCB.

The bonding is of great importance. Bad bonding can result in grounding plates which are not perfectly grounded and transmit electro-magnetic waves which will sabotage the experiment. If the transmission line is not bonded with care, no microwaves can be induced. After this step is completed, the PCB can be fixed on a probe holder.

4.2 Measurement Technique

To reduce noise and achieve superconducting properties, the microchip is cooled down to 4.2K. It is therefore inserted in a dipstick and inserted into liquid helium. By introducing the stick the temperature in the basin raises and the pressure increases, which is why the stick had to be induced slowly. Stainless steel coaxial cables which are mounted on the probe holder, on which the microchip is fixed, are leading out of the liquid helium basin and can then be connected to a measuring device. Each of the designed ring resonator chips has two ports. Each port can be used to measure transmission and induce waves at certain frequencies.

Before the measurement could begin the system was calibrated. The measuring device was a Vector Network Analyzer. The coaxial cables have to be plugged in carefully and in a precise manner to avoid reflections at the transition. Now each of the ports on the microchip can be read in- and out via the Vector Network Analyzer, and transmission from one port to the other could easily be measured. Since the resonator is placed symmetrically between the two ports, a distinction between measuring from A to B and B to A is not necessary, but has been checked. To actually calibrate the system the coaxial cable is not connected to the two ports directly. Not passing through the resonator, going directly from port A to B, absorption by imperfection and other environmental influences can be measured and later be extracted from the actual measurement.

5 Results

5.1 Calibration

As explained in section 4.2 on the previous page, the system was first calibrated. Its absorption at the indicated frequencies can be obtained from figure 9.

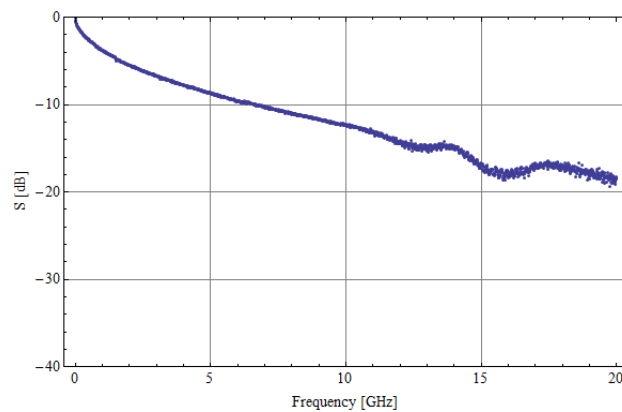


Figure 9: Calibration data

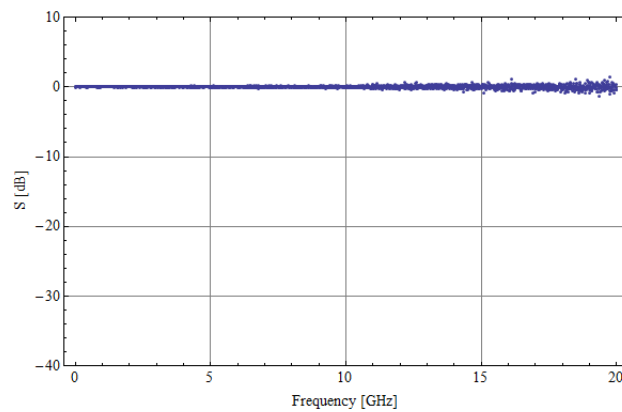


Figure 10: Interpolated subtracted from raw calibration data

Since the measurement was set up to measure 20'000 data points, without dependence of the measurement interval, the calibration data was interpolated using the *Wolfram Mathematica* build in interpolation function of 3rd grade polynomials. The effect of the interpolation can be seen in

figure 10, where the interpolated calibration data was subtracted from the raw data.

5.2 Resonator

Due to the static recording of 20'000 data points, the scale of the measurements has been varied to measure significant regions with a higher measurement density. An uncalibrated and calibrated measurement is shown in figure 11.

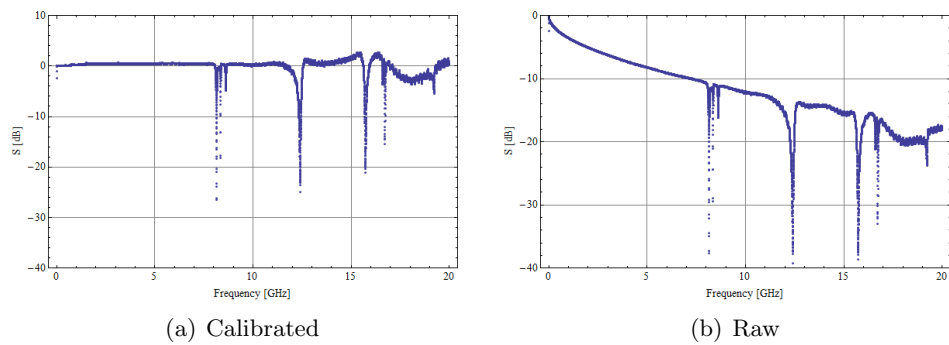
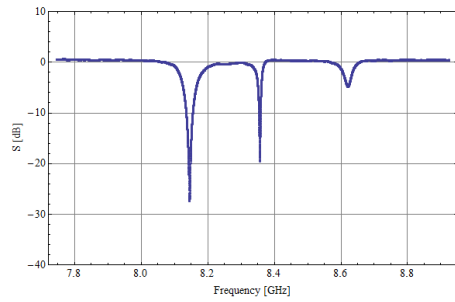


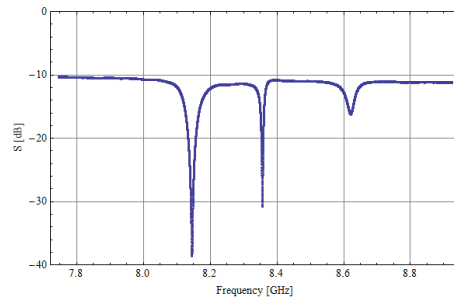
Figure 11: Resonator frequency absorption

The calibrated spectrum actually shows an increased transmission relative to the input frequencies, a property that cannot stem from the resonator. A more precise calibration and measurement could possibly improve the data.

In general five absorption peaks can be seen around 8,12,16,17 and 19 GHz. The last peak though is relatively small compared to the others. We can see that some peaks appear in groups. We will refer to them as peak cluster and to the other as single peaks. The calibrated close-up of the five significant regions is illustrated in the figures 12,13,14,15 and 16.

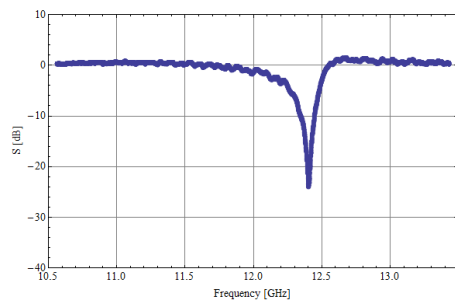


(a) Calibrated

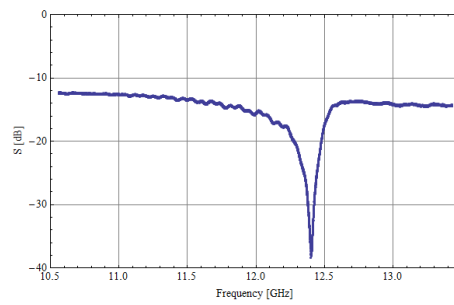


(b) Raw

Figure 12: First Peaks

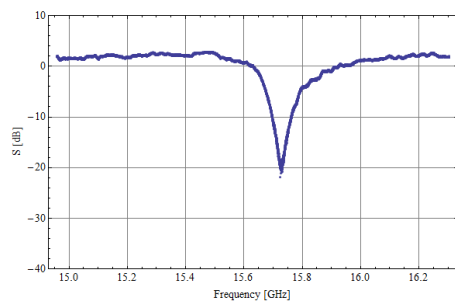


(a) Calibrated

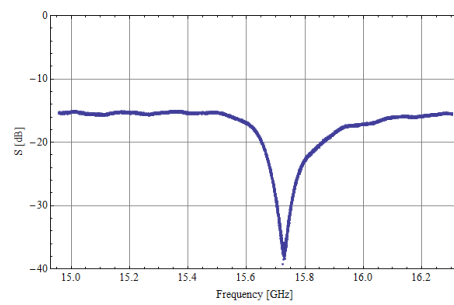


(b) Raw

Figure 13: Second Peaks



(a) Calibrated



(b) Raw

Figure 14: Third Peaks

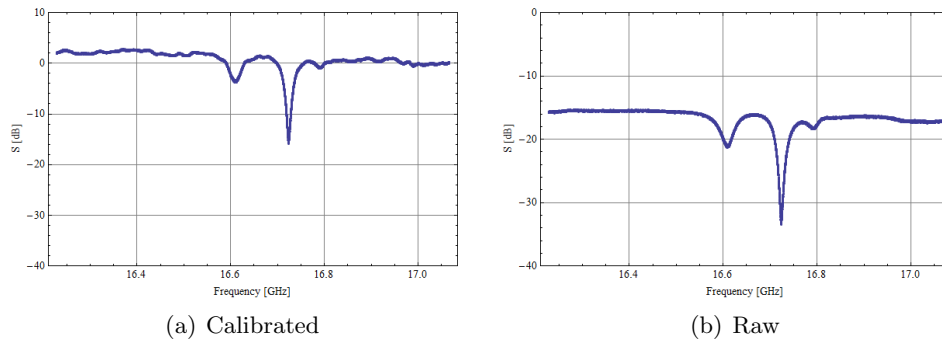


Figure 15: Fourth Peaks

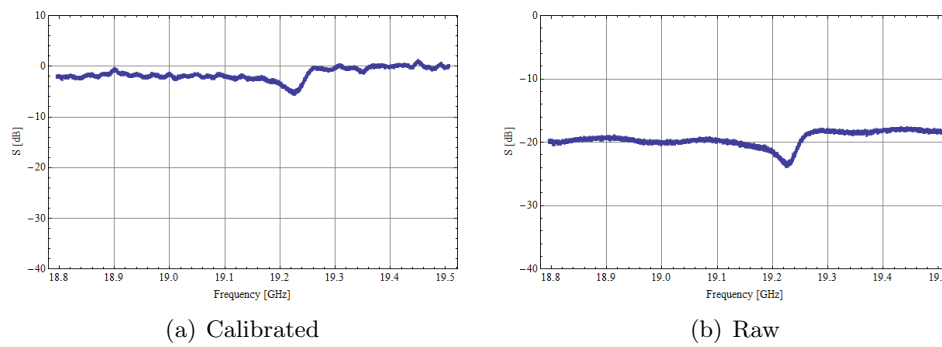


Figure 16: Fifth Peaks

When comparing the peaks at higher resolution the existence of not one, but many peaks is exposed in figure 12 and 15 on the preceding page. In the latter, the middle peak appears to have the strongest breakout, whereas in the first one the peaks become successively smaller. A comparison of the peak clusters 1 and 4 yields no connection between the two, as can be seen in table 3 and figure 17. There the absorption peaks have been plotted with the relative frequency difference to the first absorption peak in the cluster. The first peak of each cluster has been set to lay at 0.1 GHz. Also notable is the fact, that only some regions consist of a cluster of peaks.

	Resonance [GHz]	Peak Absorption [mW]
Peak 1,1	8.14684	1.11332
Peak 1,2	8.35538	1.02144
Peak 1,3	8.61993	0.771722
Peak 4,1	16.6109	1.08424
Peak 4,2	16.7246	1.38214
Peak 4,3	16.7906	0.34701

Table 3: Peak Comparison Data

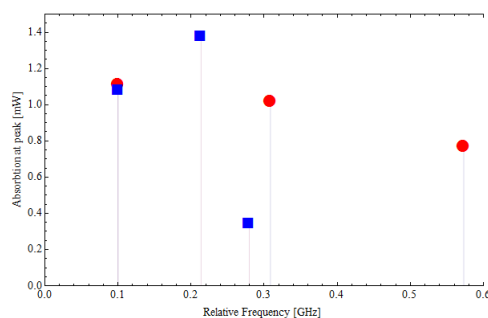


Figure 17: Peak Comparison

The peaks were labeled from 1,1 to 5,1, the first digit corresponds to the peak cluster or single peaks and the latter to the peaks in the cluster, with 1 being at the lowest frequency. To be able to make assumptions on the resonator properties a Lorentz curve was fitted to each of the peaks. The q-factors could so be determined and have been written to table 4 and 5 on the following page. Difficulties arose especially when fitting the curve to asymmetric and small q-factor peaks, namely peaks 2,1 and 3,1 (see fig. 18).

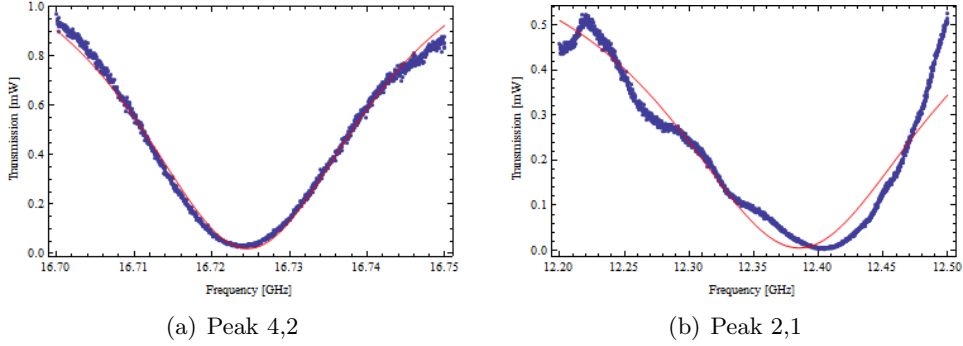


Figure 18: Red: Fitted Lorentzian curve

Measurement	Peak 1,1	Peak 1,2	Peak 1,3	Peak 2,1
Raw				
Q-factor	143.181	553.349	227.792	34.7349
Frequency [Ghz]	8.14791	8.35546	8.6199	12.3365
Min [dB]	-29.5306	-31.1152	-16.1753	-28.6436
FWHM [Ghz]	0.0284532	0.0075499	0.0189205	0.17758
Calibrated				
Q-factor	131.581	536.877	243.421	50.3229
Frequency [Ghz]	8.14684	8.35538	8.61993	12.3849
Min [dB]	-27.0676	-17.1454	-4.88862	-22.652
FWHM [Ghz]	-0.0309575	0.00778147	-0.0177058	-0.123055

Table 4: Measured Peak Data (Peaks 1-3)

Measurement	Peak 3,1	Peak 4,1	Peak 4,2	Peak 4,3	Peak 5,1
Raw					
Q-factor	52.6532	396.459	430.939	590.97	521.51
Frequency [Ghz]	15.74	16.61	16.72	16.79	19.22
Min [dB]	-31.6993	-21.295	-33.3704	-18.3515	-23.4991
FWHM [Ghz]	0.149736	0.0209462	0.0194068	0.0142064	0.01843
Calibrated					
Q-factor	82.505	440.777	452.055	776.97	475.002
Frequency [Ghz]	15.74	16.61	16.72	16.79	19.22
Min [dB]	-23.5283	-3.9471	-16.9406	-0.94434	-5.20175
FWHM [Ghz]	0.0954063	-0.0188428	-0.0184984	0.0108052	-0.0202326

Table 5: Measured Peak Data (3-5)

6 Discussion

In figure 19 the absorption line of the RR500d4 Resonator is shown a) as simulated, b) as measured.

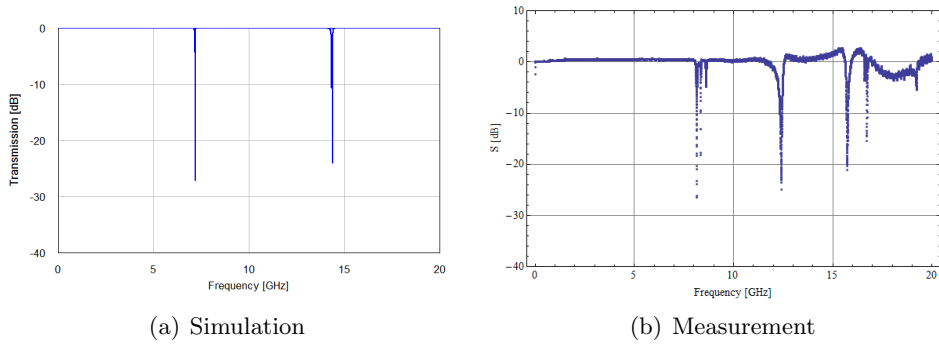


Figure 19: Comparison between Simulation and Measurement

To be able to compare both lines better, the peaks have been plotted together in figure 20.

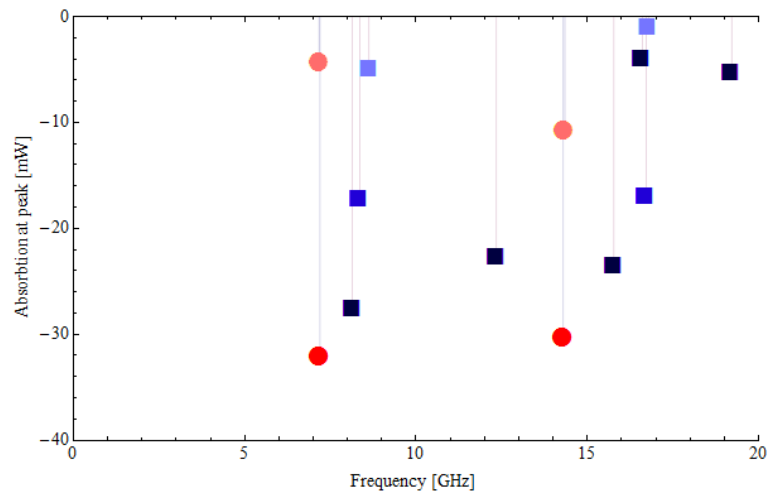


Figure 20: Peak Absorptions. Red round markers: Simulation, Quadratic blue markers: Measurement, (exists a cluster of peaks the brightness of makers is decreasing with frequency)

Clearly no connection between the two graphs can be found. We have

1. Resonance frequencies at different wavelengths

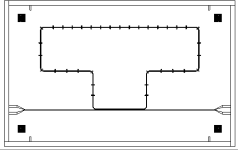
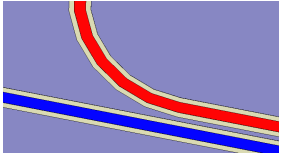
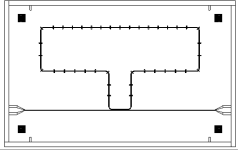
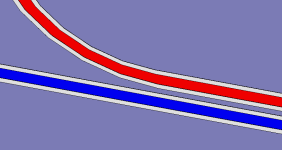
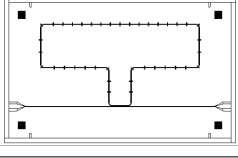
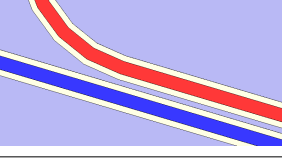
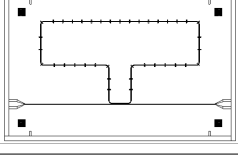
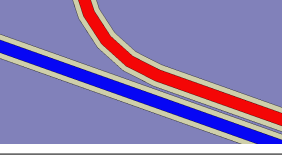
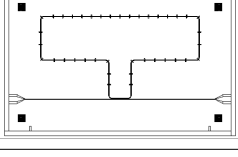
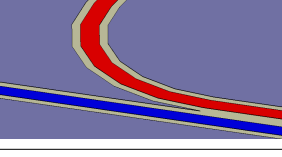
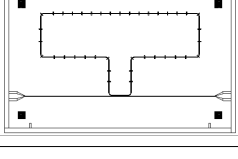
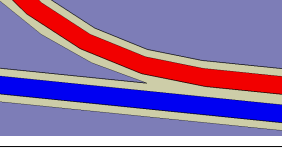
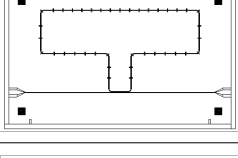
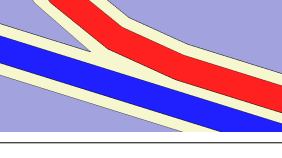
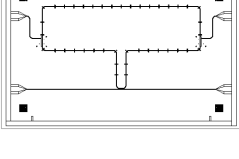
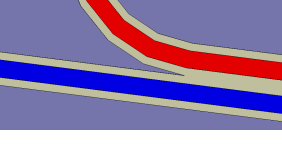
2. Absorption strengths at different levels
3. Equidistant resonance frequencies in the simulation, randomness in the measurement
4. Resonance peaks which appear in groups of up to two in the simulation, whereas up to three in the measurement
5. Peaks lying close to one another in simulation and measurement differ greatly by q-factors

7 Conclusion

In this thesis various coplanar ring resonator have been designed, fabricated and been analyzed experimentally. The measurement of the one tested ring resonator has shown, that it cannot be modeled in absorption behavior with the assumptions and programs used. As shown in section 6, frequencies, Q-factors, shape and periodicity are not in compliance with the simulation. Additional bond wires, connecting the adjacent ground plates, that are surrounding the transmission lines, might allow the measurements to be more precise, since a none-zero potential, especially the ones enclosed in the ring resonator might have a great influence on the results.

Nevertheless the behavior of the resonator is quite fascinating, especially the unforeseen existence of triple peak clusters. It would be interesting to see how those, and the whole absorption structure, envelope by measuring alike ring resonators. An explanation is, right now, hard to tell, since only one resonator has been measured and no assumptions on tendencies or trends of those effects can be made.

A Designed Resonators

Description	Schematic	Coupling
RR1500i4 17180 μm total length 1500 μm couple length 4 μm barrier width coupled through barrier		
RR500i5 17180 μm total length 500 μm couple length 5 μm barrier width coupled through barrier		
RR500i4 17180 μm total length 500 μm couple length 4 μm barrier width coupled through barrier		
RR500i2 17180 μm total length 500 μm couple length 2 μm barrier width coupled through barrier		
RR500d9 17180 μm total length 500 μm couple length 9 μm couple distance coupled directly		
RR500d6 17180 μm total length 500 μm couple length 6 μm couple distance coupled directly		
RR500d4 17180 μm total length 500 μm couple length 4 μm couple distance coupled directly		
RR100d9 17180 μm total length 100 μm couple length 9 μm couple distance coupled directly		

References

- [1] Richard Feynman. Simulating physics with computers. *International Journal of Theoretical Physics*, 21(6):467–488, 1982.
- [2] L M K Vandersypen, M Steffen, G Breyta, C S Yannoni, M H Sherwood, and I L Chuang. NMR quantum computing: Realizing Shor’s algorithm. *Nature*, 414:883–887, 2001.
- [3] Alexandre Blais, Ren-Shou Huang, Andreas Wallraff, S M Girvin, and R J Schoelkopf. Cavity quantum electrodynamics for superconducting electrical circuits: an architecture for quantum computation. *Physical Review A*, 69(6):14, 2004.
- [4] R Simons. *Coplanar waveguide circuits, components, and systems*, volume 7. John Wiley and Sons, 2001.
- [5] Bahaa E A Saleh and Malvin Carl Teich. *Fundamentals of Photonics*, volume 5 of *Wiley Series in Pure and Applied Optics*. Wiley, 1991.
- [6] M A Popovic, Christina Manolatou, and Michael R Watts. Coupling-induced resonance frequency shifts in coupled dielectric multi-cavity filters References and links. *Optics Express*, 14(3):1208, 2006.
- [7] M Göppl, A Fragner, M Baur, R Bianchetti, S Filipp, J M Fink, P J Leek, G Puebla, L Steffen, and A Wallraff. Coplanar Waveguide Resonators for Circuit Quantum Electrodynamics. *Journal of Applied Physics*, 104(11):8, 2008.